Res Chem Intermed (2017) 43:3677–3690
DOI 10.1007/s11164-016-2835-x

Environmentally benign chitosan as precursor and reductant for synthesis of Ag/AgCl/N-doped carbon composite photocatalysts and their photocatalytic degradation performance

Yuhan Wu[1] · Shanshan Chen[1] · Xuhong Guo[1,2] · Jianning Wu[1] · Banghua Peng[1] · Zhiyong Liu[1]

Received: 10 May 2016 / Accepted: 16 December 2016 / Published online: 27 December 2016

Abstract In this study, we reported a novel Ag/AgCl loaded N-doped carbon composite photocatalyst (Ag/AgCl/NC) which was fabricated by a facile and green method. The composite was prepared only by two simple steps. Firstly, the Ag/N-doped carbon (Ag/NC) was prepared by one-step hydrothermal treatment; during this progress the environmentally benign and renewable natural chitosan was used as not only reducer and stabilizer, but also as a nitrogen source and carbon source. Secondly, Ag/AgCl/NC composite was synthesized via in situ oxidation reaction by adding $FeCl_3$. The Ag/AgCl/NC composite was characterized using X-ray diffraction, transmission electronic microscopy, energy dispersive X-ray spectra, UV-visible diffused reflectance spectra, X-ray photoelectron spectroscopy and nitrogen adsorption-desorption measurements, respectively. The obtained Ag/AgCl/NC composite exhibited a superior photocatalytic activity and stability for the degradation of rhodamine B (RhB) under visible light irradiation.

Keywords N-doped carbon · Ag/AgCl · Surface plasmon resonance · Chitosan · Photocatalysis

✉ Zhiyong Liu
lzyongclin@sina.com

[1] School of Chemistry and Chemical Engineering, Key Laboratory of Materials-Oriented Chemical Engineering of Xinjiang Uygur Autonomous Region, Engineering Research Center of Materials-Oriented Chemical Engineering of Xinjiang Bingtuan, Shihezi University, Shihezi 832003, People's Republic of China

[2] State Key Laboratory of Chemical Engineering, East China University of Science and Technology, Shanghai 200237, People's Republic of China

Introduction

With the rapid development of human society, the environmental problem caused by organic contaminants is increasingly serious. If the organics cannot be properly treated, they may threaten the health of human and animals [1, 2]. Conventional technologies, adsorption, coagulating sedimentation, electro-coagulation, membrane filtration, and ozonation, are always ineffective, costly and disadvantaged [3–5]. Recently, photocatalysis technology as a "green" and promising method has received extensive attention [4, 6]. Among the various semiconductor photocatalysts, TiO_2 has attracted extensive attention, due to its cheap, nontoxic, abundant, high photocatalytic activity and chemical stability [1, 7, 8]. Unfortunately, TiO_2 can only respond to UV light (only accounts for $\sim$5% of the total solar spectrum) because of its large band gap (3.2 eV). However, visible light energy accounts for $\sim$48% of the solar energy, which is far more abundant than UV light [9]. Therefore, the development of visible light responding photocatalysts has obtained extensive research.

Recently, Ag/AgX (X = Cl, Br, I) photocatalysts have been demonstrated to have a kind of promising visible light response photocatalysts due to the surface plasmon resonance (SPR) of Ag nanoparticles (NPs) [8, 10, 11]. However, Ag/AgX photocatalysts still have some problems, for example, Ag/AgX nanoparticles are easily aggregated into micrometer-sized particles, and there is the short lifetime of photogenerated electron-hole pairs [12, 13]. One good strategy to solve the problem of aggregation and/or enhance the photocatalytic activities is immobilizing Ag/AgX photocatalysts on/into various support materials, such as carbonaceous materials [2, 14–17], inorganic clays [4, 13, 18], Al_2O_3 [19, 20], mordenite [21], MCM-41 [22], MOF [12], and silica [23, 24]. Among these support materials, carbonaceous materials had been intensively studied, because they possess many advantages, such as cheapness, safety, corrosion resistance, high mechanical strength, and electrical and chemical properties [25–27]. An et al. [16] described the synthesis of Ag/AgX-CNTs nanocomposite photocatalysts using an ultrasonic assistant deposition–precipitation method at room temperature. This kind of photocatalysts exhibited excellent photocatalytic activity for removing 2,4,6-tribromophenol. Zhang et al. [17] successfully fabricated an Ag/AgCl-activated carbon composite by an impregnation-precipitation-reduction method. This material possessed satisfactory photocatalytic activity for methyl orange and phenol under visible light. Yu et al. [28] reported the preparation of Ag/AgCl-reduced graphene oxide (rGO) via a facile reduction-reoxidization route. The photocatalytic experimental results showed that the nanocomposite had a much higher rate constant than the Ag/AgCl. In addition, it had been demonstrated in much previous research that nitrogen-doping can effectively enhance the electric, optical and mechanical properties. Furthermore, nitrogen-doping can increase the number of chemically active sites, this is in favour of improving the dispersion of nanoparticles and the much higher resistance to nanoparticles agglomeration and coarsening [1, 25, 26]. Hu et al. [29] had successfully prepared 2-D sandwich-like CdS nanoparticles/nitrogen-doped rGO hybrid nanosheets by a surface-layer-absorption strategy combined with an in situ

sulfdation reaction route. The CdS/N-rGO composites possessed higher photoelectrochemical current response and photocatalytic activity than pure CdS and CdS/rGO. Zhou et al. [1] synthesized Ag_2O/N-doped helical carbon nanotubes with the coprecipitation method. The Ag_2O/N-doped helical carbon nanotubes exhibited high and stable catalytic activity. However, the traditional methods (e.g., chemical vapour annealing, wet dipping process) to prepare N-doped carbon always need very harsh and multistep processes. The general nitrogen sources, such as ammonia, amines, and urea, are less sustainable and available [30]. So to develop a facile synthetic method with stable and nontoxic nitrogen sources to prepare N-doped carbon is fascinating and significant.

Chitosan is a hydrophilic and cationic biopolymer produced by partial N-deacetylation of chitin, which is the second most plentiful natural biopolymer in the world after cellulose [31]. Chitosan can adsorb and chelate metal ions due to it containing a great many hydroxyl (-OH) and amino (-NH_2) groups [30, 32]. It also exhibits many excellent properties, such as biodegradability, biocompatibility and antibacterial properties [33, 34]. At the same time, many works demonstrated that chitosan can serve as a reducing and stabilizing agent to prepare noble metallic nanoparticles [33–35] and transform into N-doped carbon material directly [30, 36].

Until now, to the best of our knowledge, chitosan as precursor and reductant to synthesis Ag/AgCl/NC composite photocatalyst had not been studied yet and Ag/AgCl was firstly loaded on N-doped carbon. In this study, the composite was prepared only by two simple steps. Firstly, Ag/NC composite was obtained only by one-step hydrothermal treatment, which was firstly reported by our group [37]. In this process, chitosan was used to reduce silver precursor to Ag NPs and resist Ag NPs agglomeration, therefore, any other strong reducing and protecting agents were not needed. Moreover, the nitrogen source was not additionally added, chitosan not only served as a carbon source, but also acted as a nitrogen source. Secondly, Ag/AgCl NPs were formed by in situ redox reaction between Ag and $FeCl_3$ [38–40]. The experimental results demonstrated that the Ag/AgCl NPs were successfully anchored on N-doped carbon and Ag/AgCl/NC composite photocatalysts exhibited superior photocatalytic activity and stability for the degradation of rhodamine B under visible light.

Experimental section

Materials

Chitosan flakes (Practical grade, >90.0% deacetylated; viscosity, <100 cps) were purchased from Shanghai Lanji Technological Development Co., Ltd. Silver nitrate (99.8%) and ferric chloride (99.0%) were purchased from Xi'an Chemical Reagent Factory. Anhydrous ethanol was obtained from Tianjin Fuyu Fine Chemical Reagent Company. Rhodamine B was purchased from Tianjin Guangfu Fine Chemical Research Institute Reagent Factory. All the reagents are analytical grade and without further purification.

Synthesis

The synthesis procedure of Ag/AgCl/NC composite is illustrated in Scheme 1.

Synthesis of Ag/NC composite

Ag/NC composite was prepared via a one-step hydrothermal progress based on our previous work [37]. Briefly, 0.5 g chitosan flakes were dispersed in 40 mL $AgNO_3$ solution (0.05 M). The mixture was sonicated for 10 min, and then transferred into a Teflon-lined autoclave and kept at 180 °C for 12 h. After the reactor was cooled to room temperature, the black products were washed with deionized water and anhydrous ethanol for several times and dried in a vacuum oven at 50 °C overnight.

Synthesis of Ag/AgCl/NC composite

The Ag/AgCl/NC composite was prepared by an in situ oxidation method. Typically, 0.1 g as-prepared Ag/NC composite was added into 20 mL at a certain concentration of $FeCl_3$ (12.5, 25.0, 50.0 and 100 mM) under stirring at room temperature. After stirring for 4 h, the obtained samples were washed with deionized water and anhydrous ethanol for several times. Finally, the Ag/AgCl/NC composites were dried in a vacuum oven at 50 °C overnight. The as-prepared samples were denoted as S1, S2, S3 and S4, respectively.

Characterizations

The crystal structures and phase data of the prepared samples were collected by using an X-ray diffractometer (Bruker D8-Advance, Germany) with CuKa radiation in the 2θ range of 10°–90°. The morphological features and composition of the as-

Scheme 1 Synthesis of Ag/AgCl/NC composites

prepared Ag/AgCl/NC composites were obtained by transmission electron microscope (TEM, Tecnai G2 F20) and an energy dispersive X-ray spectrometer (EDX). X-ray photoelectron spectroscopy (XPS) was performed using an Axis Ultra spectrometer with a monochromatized Al-Kα X-ray as excitation source (225 W). UV-vis absorption spectra were recorded by an UV-visible spectrophotometer (UV-2450, Shimadzu Corporation, Japan). Nitrogen adsorption-desorption measurements was determined by using a Micromeritics ASAP 2020 nitrogen adsorption apparatus (USA).

Photocatalytic activity

The photocatalytic activities of the prepared composites were evaluated by the degradation of RhB under visible light. In a typical procedure for photocatalytic experiments, aqueous suspensions of RhB (50 mL, with an initial concentration of 10 mg/L) and composite powder (20 mg) were placed in a quartz vessel. Prior to photocatalytic reaction, the mixture was stirred in the dark for 2 h to establish an adsorption-desorption equilibrium. After that, the mixture was placed under a 250 W Xe lamp equipped with a UV cutoff filter ($\lambda > 420$ nm) and keeping the distance between the center of the quartz vessel and the lamp at about 20 cm. Then turning on the light, the suspension (about 2 mL) was taken from the mixture at every 10 min and centrifuged at 5000 rpm for 5 min to remove the composite photocatalyst. The concentration of upper clear liquid was determined by UV-vis spectrophotometer (TU-1901, Beijing, China).

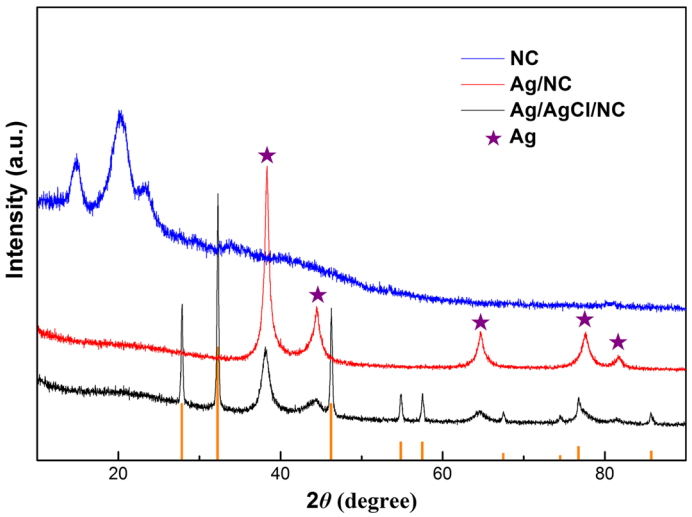

Fig. 1 XRD patterns of NC, Ag/NC and Ag/AgCl/NC

Results and discussion

Photocatalyst characterization

In order to determine the phase structure and crystallinity of the prepared samples, XRD analysis was carried out. As shown in Fig. 1, comparing Ag/NC (red line) with NC (blue line), there were five new characteristic diffraction peaks ($2\theta = 38.28°$, 44.39°, 64.60°, 77.50° and 81.70°) that can be clearly observed, which corresponded to the (111), (200), (220) (311) and (222) crystalline silver reflection of the face-centered lattice of silver (JCPDS No. 04-0783). Therefore, it can be proved that silver ions were successfully reduced to metallic silver. After the metallic silver was oxidized by $FeCl_3$, all the diffraction peaks could be indexed to the typical cubic phase of AgCl (orange lines, JCPDS No. 31-1238), which indicated the formation of AgCl crystals on the surface of the metallic silver.

The microstructures of the Ag/AgCl/NC composite were studied by TEM (Fig. 2). In Fig. 2a, it can be seen that after hydrothermal treatment, numerous dark Ag NPs were anchored on NC. In this process, chitosan acted as a reducer which successfully reduced silver ions to metallic silver and also as protecting agent to

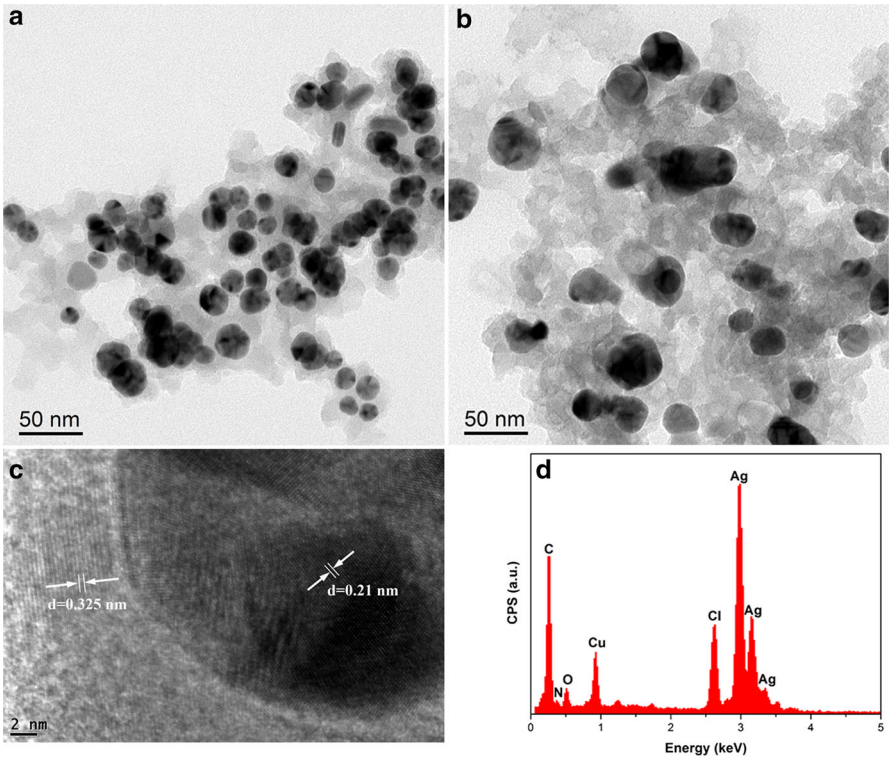

Fig. 2 **a**, **b** TEM images of Ag/NC and Ag/AgCl/NC; **c** HRTEM of the Ag/AgCl/NC, **d** EDX spectrum of Ag/AgCl/NC

resist the agglomeration of Ag NPs. For Ag/AgCl/NC composite, the around of Ag NPs had a light black AgCl layer (Fig. 2b). Figure 2c shows the typical HRTEM image of Ag/AgCl/NC, the distinct lattice fringes of $d = 0.325$ and 0.21 nm, which match with the (111) plane of AgCl and the (111) plane of Ag. Energy-dispersive X-ray spectroscopy was used for identifying the composition of Ag/AgCl/NC. From Fig. 2d, the peaks of C, N, O, Ag and Cl were attributed to the Ag/AgCl/NC composite. Combining this supportive evidence with XRD analysis, it can be determined that Ag/AgCl/NC composite was successful prepared. The Cu signal can be assigned to the grid used in the TEM measurement.

More detailed information of the surface elemental compositions and bonding environment of the Ag/AgCl/NC composite were analyzed by X-ray photoelectron spectroscopy. Figure 3a displays the fully scanned spectra in the range of 0–1000 eV. The characteristic signals of C, N, O, Ag and Cl can be clearly seen. The N 1*s* peak of Ag/AgCl/NC can be deconvoluted into three peaks at 398.4, 399.5 and 400.4 eV, which were assigned to pyridinic-type N, amino-type N and pyridinium nitrogen of condensed polycycles (Fig. 3b) [41, 42]. The XPS high-resolution spectrum of Ag 3*d* (Fig. 3c) had two individual peaks at about 373.0 and 367.0 eV, which can be attributed to Ag $3d_{3/2}$ and Ag $3d_{5/2}$. The Ag $3d_{3/2}$ peak can be divided into two different peaks at 373.6 and 372.7 eV, and the peak of Ag $3d_{5/2}$ can be divided into 367.6 and 366.7 eV. The peaks at 373.6 and 367.6 eV were

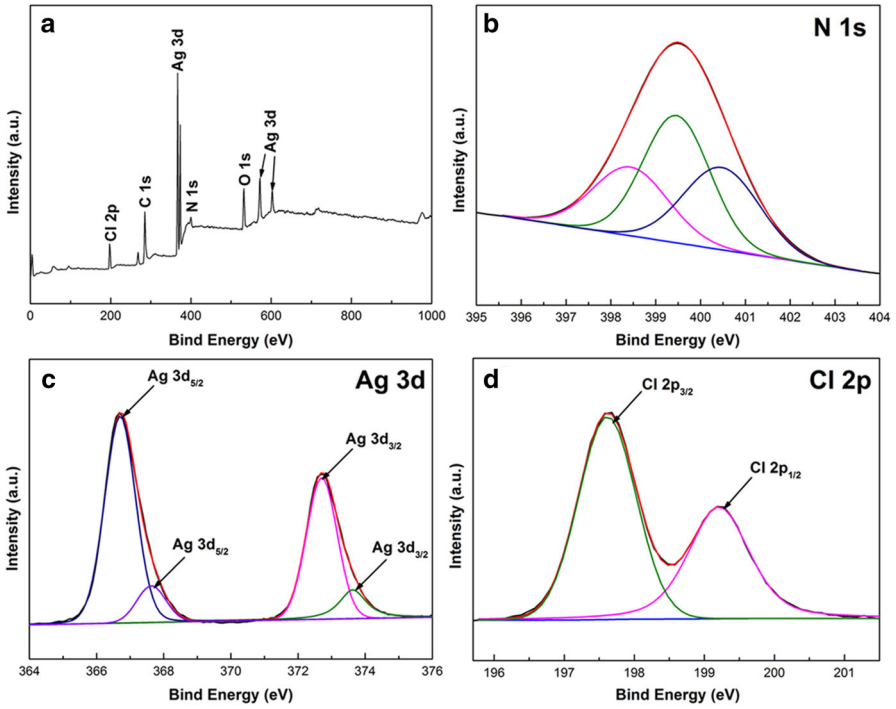

Fig. 3 **a** XPS fully scanned spectra of the Ag/AgCl/NC, **b–d** High-resolution XPS spectra of N 1*s*, Ag 3*d* and Cl 2*p*

assigned to metallic silver, and the peaks at 373.7 and 366.7 eV correspond to Ag^+ of AgCl [43]. In Fig. 3d, the Cl species displays two peaks at about 197.6 and 199.2 eV, which correspond to Cl $2p_{3/2}$ and Cl $2p_{1/2}$, respectively.

The photoabsorption abilities of NC, Ag/NC and Ag/AgCl/NC were measured by UV-vis diffuse reflectance spectra, as shown in Fig. 4. The Ag/NC composite exhibited the high absorption ability in the visible light region, which can be attributed to the surface plasmonic resonance effect of Ag NPs [39, 44]. In spite of the light absorption ability of Ag/AgCl/NC obviously decreasing compared to Ag/NC, it still possessed the high absorption ability in both UV and visible light regions; this was beneficial to efficiently utilize the sunlight.

Photocatalytic activity and mechanism

The photocatalytic performances of the Ag/AgCl/NC composite photocatalysts were evaluated by degradation of RhB under visible light irradiation ($\lambda > 420$ nm) (Fig. 5a). For comparison, the photodegradation of RhB with AgCl and Ag/NC was also investigated. During the adsorption process, all the Ag/AgCl/NC composites exhibited a high adsorption capacity for the RhB solution, which was beneficial to the photocatalytic degradation of organic contaminants [4]. This phenomenon can be attributed to the high specific surface area of Ag/AgCl/NC composite (the BET specific surface area of S3 is as high as 54.31 m^2/g, as shown in Fig. 6). After the light was turned on, the degradation of RhB progressed steadily, and all the composite photocatalysts exhibited excellent catalytic performances. The photocatalytic performance enhanced as the concentration of $FeCl_3$ (below 50.0 mM) increased, when the concentration reached 50.0 mM, the composite photocatalyst (sample S3) had the highest photocatalytic activity. Further increases of the concentration (sample S4) caused the photocatalytic activity to decrease. According to previous reports, the photocatalytic activity was highly dependent on the ratio of

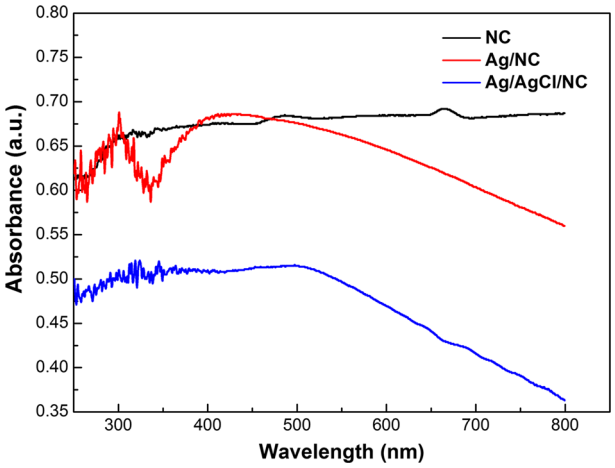

Fig. 4 UV-vis diffuses reflectance spectra of the NC, Ag/NC and Ag/AgCl/NC

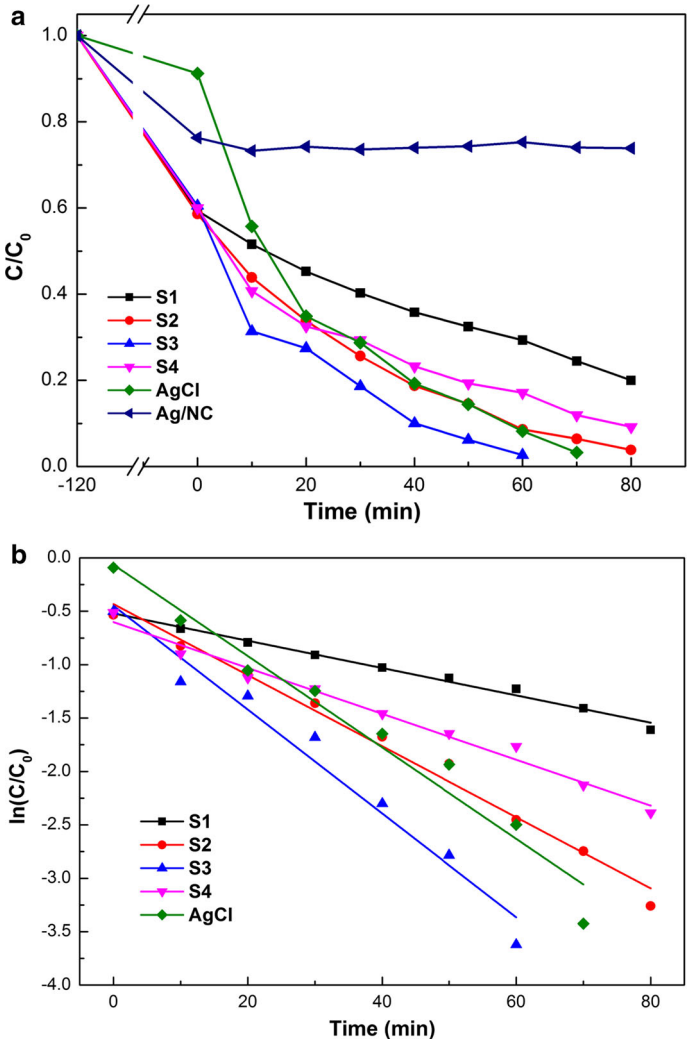

Fig. 5 **a** Effect of visible light for different sample on degradation of RhB ($C_0 = 10$ mg/L); **b** Plots of $\ln(C/C_0)$ versus irradiation time for the degradation of RhB solution under visible light irradiation

Ag and $FeCl_3$, different molar ratios of Ag and $FeCl_3$ may lead to the changes of the product in composition, microstructure, and morphology [39, 45]. The in-depth action clearly needs to be further investigated. We also tested the photocatalytic activities of Ag/NC and pure AgCl. Ag/NC displayed excellent adsorbability, but did not have any photocatalytic performance, while AgCl possessed the desired activity.

We also investigated the reaction kinetics of RhB photodegradation by the as-prepared composite photocatalysts. It had been demonstrated that the photocatalytic degradation process follows the Langmuir-Hinshelwood first-order kinetic model at

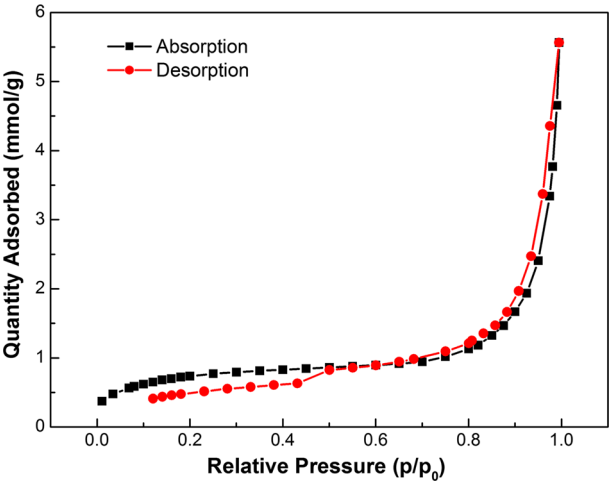

Fig. 6 N_2 adsorption-desorption isotherm of S3

low dye concentration [31]. The rate constant (k) for the photocatalytic degradation of RhB under visible light irradiation can be analyzed by the equation as below:

$$\ln (C/C_0) = kt,$$

where C and C_0 were the time-dependent and initial ($t = 0$) concentration of the RhB, and k was the apparent first-order rate constant (min^{-1}). The kinetic plots of S1–S4 are depicted in Fig. 5b. The reaction rate constants (k) were calculated to be 0.0128, 0.0333, 0.0486, 0.0215 and 0.0428 min^{-1} for S1, S2, S3, S4 and pure AgCl. This result demonstrated that the sample S3 had the highest photocatalytic activity for RhB. Although pure AgCl possesses a similar effect, however, it is worth pointing out that the amount of Ag/AgCl in Ag/AgCl/NC is much less than pure AgCl. Therefore, the 50.0 mM was considered as the optimal concentration. Photocatalytic degradation performance for RhB of some other photocatalysts, reported in the literature, is reported in Table 1. It shows that the Ag/AgCl/NC composite photocatalyst possessed a relatively desired photocatalytic activity. There were two reasons for the highly photocatalytic performance of composites. (1) In the process of Ag/NC preparation, NC effectively prevented Ag NPs agglomeration. Furthermore nitrogen doping improved carbon-metal binding and increased the number of chemically active sites. This means that Ag/AgCl NPs can possess the smaller particle size and larger special surface area, and this was beneficial to provide more active sites in contact with RhB [26]. (2) The synchronous role of adsorption and photocatalytic activity of the Ag/AgCl/NC composites [4, 17].

It was worth noting that the stability of the photocatalyst was important for practical applications. The stability of the Ag/AgCl/NC composite photocatalyst (S3) and pure AgCl were further evaluated by RhB degradation tests for three cycle reactions, the relevant experimental results are shown in Fig. 7. The results verified that both the Ag/AgCl/NC composite photocatalyst and pure AgCl had high photocatalytic activities in the first run. However, the photocatalytic activity of pure

Table 1 The comparison of photocatalytic degradation performance for RhB in this paper with other photocatalysts from the literature

Reference	Photocatalyst	Dosage of photocatalyst (mg)	Concentration of RhB (mg/L)	Volume of RhB (mL)	Light source	k
This work	Ag/AgCl/NC	20	10	50	250 W Xe lamp	0.0486 min^{-1}
[46]	α-Fe_2O_3@Ag/AgCl	3	10	10	300 W mercury lamp	0.0276 min^{-1}
[47]	Ag_2CO_3/Ag/AgBr	5	20	20	500 W Xe lamp	0.098 min^{-1}
[48]	Ag@Ag_3PO_4/RGO	60	12	30	450 W Xe lamp	0.1699 min^{-1}
[49]	Ag_3VO_4/g-C_3N_4	50	5	100	400 W metal halide lamp	0.0556 min^{-1}
[50]	Ag@AgCl/$K_2Ti_4O_9$	250	10	250	250 W metal halide lamp	0.030 h^{-1}
[51]	Gd_2O_3/Ag_3VO_4	–	10	150	150 W tungsten halogen lamps	0.0261 min^{-1}
[52]	Ag_3PO_4/SBA-15	100	30	100	300 W Xe arc lamp	0.166 min^{-1}

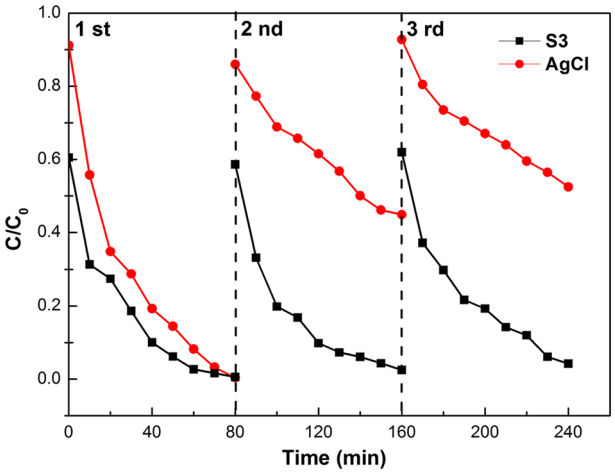

Fig. 7 The cycling runs of the degradation of RhB over S3 and AgCl

AgCl dramatically decreased after the first run, this is due to that AgCl is photosensitive, a certain amount of Ag^{+} was photoreduced to Ag^{0}. On the contrary, the photocatalytic activity of S3 slightly decreased, but still kept a high efficiency.

On the basis of the results of previous work [53], the mechanism was proposed for the dye photodegradation over the Ag/AgCl/NC composite. Silver nanoparticles absorbed visible light photons, and then generated electron–hole pairs. Induced from the surface plasmon resonance, the electron–hole pairs can be separated efficiently. The electron can react with molecular oxygen to generate a super oxide radical $\left(\cdot O_2^-\right)$, while the Cl^- combined hole can generate a Cl^0 atom. $\cdot O_2^-$ and Cl^0 as reactive a radical species can oxidize RhB and then Cl^0 is reduced to Cl^- again.

Conclusion

In this work, a novel visible-light-driven plasmonic Ag/AgCl loaded N-doped carbon composite photocatalyst was successfully synthesized by a relatively green and simple method. Renewable natural chitosan acts as a reducer, stabilizer, nitrogen source and carbon source to prepare Ag/AgCl/NC precursors by one-step hydrothermal treatment. Subsequently, AgCl was formed via in situ oxidation reaction with $FeCl_3$. The photocatalytic experimental results indicated that 50.0 mM was the optimal concentration of $FeCl_3$. The composites exhibited excellent photocatalytic activity and high stability. The enhanced photocatalytic activity of Ag/AgCl/NC can be attributed to the synergy of excellent adsorbability and photocatalytic activity, moreover, the smaller particle size of Ag/AgCl can provide more surface active sites for the decomposition of organic substances. This work may provide an easy way to prepare visible light photocatalytic materials.

Acknowledgements This work was supported financially by funding from the National Natural Science Foundation of China (21367022), Bingtuan Innovation Team in Key Areas (2015BD003).

References

1. J.J. Xue, S.S. Ma, Y.M. Zhou, Z.W. Zhang, X. Wu, C.G. She, RSC Adv. **5**, 3122 (2015)
2. M.S. Zhu, P.L. Chen, M.H. Liu, Langmuir **28**, 3385 (2012)
3. S.F. Kang, Y. Fang, Y.K. Huang, L.-F. Cui, Y.Z. Wang, H.F. Qin, Y.M. Zhang, X. Li, Y.G. Wang, Appl. Catal. B Environ. **168–169**, 472 (2015)
4. Y.Q. Yang, G.K. Zhang, Appl. Clay Sci. **67–68**, 11 (2012)
5. L. Shi, L. Liang, J. Ma, Y.N. Meng, S.F. Zhong, F.X. Wang, J.M. Sun, Ceram. Int. **40**, 3495 (2014)
6. N. Tian, H.W. Huang, Y.H. Zhang, Appl. Surf. Sci. **358**, 343 (2015)
7. B.Z. Tian, R.F. Dong, J.M. Zhang, S.Y. Bao, F. Yang, J.L. Zhang, Appl. Catal. B Environ. **158–159**, 76 (2014)
8. Q.S. Dong, Z.B. Jiao, H.C. Yu, J.H. Ye, Y.P. Bi, CrystEngComm **16**, 8317 (2014)
9. C.H. An, W. Jiang, J.Z. Wang, S.T. Wang, Z.H. Ma, Y.P. Li, Dalton Trans. **42**, 8796 (2013)
10. C.H. An, R.P. Wang, S.T. Wang, X.Y. Zhang, J. Mater. Chem. **21**, 11532 (2011)
11. C.H. An, J.Z. Wang, J.X. Liu, S.T. Wang, Q.-H. Zhang, RSC Adv. **4**, 2409 (2014)
12. S.T. Gao, W.H. Liu, N.Z. Shang, C. Feng, Q.H. Wu, Z. Wang, C. Wang, RSC Adv. **4**, 61736 (2014)
13. X.J. Zhang, J.L. Li, X. Lu, C.Q. Tang, G.X. Lu, J. Colloid Interface Sci. **377**, 277 (2012)
14. H.J. Yu, C.J. Miller, A. Ikeda-Ohno, T.D. Waite, Catal. Today **224**, 122 (2014)
15. M.S. Zhu, P.L. Chen, M.H. Liu, ACS Nano **5**, 4529 (2011)
16. H.X. Shi, J.Y. Chen, G.Y. Li, X. Nie, H.J. Zhao, P.-K. Wong, T.C. An, ACS Appl. Mater. Interfaces **5**, 6959 (2013)
17. J.G. McEvoy, W.Q. Cui, Z.S. Zhang, Appl. Catal. B Environ. **144**, 702 (2014)
18. Sh. Sohrabnezhad, M.A. Zanjanchi, M. Razavi, Spectrochim. Acta A **13**, 129 (2014)
19. X.F. Zhou, C. Hu, X.X. Hu, T.W. Peng, J.H. Qiu, J. Phys. Chem. C **114**, 2746 (2010)
20. C. Hu, T.W. Peng, X.X. Hu, Y.L. Nie, X.F. Zhou, J.H. Qu, H. He, J. Am. Chem. Soc. **132**, 857 (2010)
21. Sh. Sohrabnezhad, A. Rezaei, Superlattices Microstruct. **55**, 168 (2013)
22. Sh. Sohrabnezhad, A. Pourahmad, Spectrochim. Acta A **86**, 271 (2012)
23. X.X. Yao, X.H. Liu, J. Mol. Catal. A Chem. **393**, 30 (2014)
24. D.X. Huy, H.-J. Lee, Y.B. Lee, W.S. Choi, J. Colloid Interface Sci. **425**, 178 (2014)
25. Z.Y. Liu, C.L. Zhang, L. Luo, Z. Chang, X.M. Sun, J. Mater. Chem. **22**, 12149 (2012)
26. X.-H. Li, M. Antonietti, Chem. Soc. Rev. **42**, 6593 (2013)
27. W.J. Lee, U.N. Maiti, J.M. Lee, J. Lim, T.H. Han, S.O. Kim, Chem. Commun. **50**, 6818 (2014)
28. P. Wang, T.S. Ming, G.H. Wang, X.F. Wang, H.G. Yu, J.G. Yu, J. Mol. Catal. A Chem. **381**, 114 (2014)
29. S.L. Wang, J.J. Li, X.D. Zhou, C.C. Zheng, J.Q. Ning, Y.J. Zhong, Y. Hu, J. Mater. Chem. A **2**, 19815 (2014)
30. L. Zhao, N. Baccile, S. Gross, Y.J. Zhang, W. Wei, Y.H. Sun, M. Antonietti, M.-M. Titirici, Carbon **48**, 3778 (2010)
31. H.Y. Zhu, R. Jiang, L. Xiao, Y.H. Chang, Y.J. Guan, X.D. Li, G.M. Zeng, J. Hazard. Mater. **169**, 933 (2009)
32. H.Y. Zhu, R. Jiang, Y.Q. Fu, Y.J. Guan, J. Yao, L. Xiao, G.M. Zeng, Desalination **286**, 41 (2012)
33. H.Z. Huang, X.R. Yang, Biomacromolecules **5**, 2340 (2004)
34. Y.F. Qiu, Z. Ma, P.A. Hu, J. Mater. Chem. A **2**, 13471 (2014)
35. D.W. Wei, W.P. Qian, Colloid. Surf. B **62**, 136 (2008)
36. A. Primo, P. Atienzar, E. Sanchez, J.M. Delgadob, H. García, Chem. Commun. **48**, 254 (2012)
37. Y.H. Wu, Z.Q. Wang, S.S. Chen, J.N. Wu, X.H. Guo, Z.Y. Liu, RSC Adv. **5**, 87151 (2015)
38. Y.P. Bi, J.H. Ye, Chem. Commun. **43**, 6551 (2009)
39. B.W. Ma, J.F. Guo, W.-L. Dai, K.N. Fan, Appl. Catal. B Environ. **130–131**, 257 (2013)
40. C. Xu, Y. Yuan, A.J. Cui, R.S. Yuan, J. Mater. Sci. **48**, 967 (2012)
41. L.-S. Zhang, X.-Q. Liang, W.-Guo Song, Z.-Y. Wu, Phys. Chem. Chem. Phys.**12**, 12055 (2009)
42. B. Xiong, Y.K. Zhou, Y.Y. Zhao, J. Wang, X. Chen, R. O'Hayre, Z.P. Shao, Carbon **52**, 181 (2013)

43. X.X. Yao, X.H. Liu, X.L. Hu, ChemCatChem **6**, 3409 (2014)
44. T. Zhou, Y.G. Xu, H. Xu, H.F. Wang, Z.L. Da, S.Q. Huang, H.Y. Ji, H.M. Li, Ceram. Int. **40**, 9293 (2014)
45. L. Sun, R.Z. Zhang, Y. Wang, W. Chen, ACS Appl. Mater. Interfaces **6**, 14819 (2014)
46. J. Liu, W. Wu, Q.Y. Tian, S.L. Yang, L.L. Sun, X.H. Xiao, F. Ren, C.Z. Jiang, V.A.L. Roy, RSC Adv. **5**, 61239 (2015)
47. J.J. Li, Y.L. Xie, Y.J. Zhong, Y. Hu, J. Mater. Chem. A **3**, 5474 (2015)
48. G. He, M. Qian, X.Q. Sun, Q. Chen, X. Wang, H.Q. Chen, Powder Technol. **246**, 278 (2013)
49. S.-Z. Wu, K. Li, W.D. Zhang, Appl. Surf. Sci. **324**, 324 (2015)
50. Y.H. Liang, S.L. Lin, J.S. Hu, L. Liu, J.G. McEvoy, W.Q. Cui, J. Mol. Catal. A Chem. **383–384**, 231 (2014)
51. G.S. Sun, H. Xu, H.M. Li, H.M. Shu, C.T. Liu, Q. Zhang, React. Kinet. Mech. Cat. **99**, 471 (2010)
52. Y.Y. Chai, L. Wang, J. Ren, W.L. Dai, Appl. Surf. Sci. **324**, 212 (2015)
53. P. Wang, B.B. Huang, X.Y. Qin, X.Y. Zhang, Y. Dai, J.Y. Wei, M.-H. Whangbo, Angew. Chem. Int. Ed. **47**, 7931 (2008)